Crystalline Actin Sheets:
Their Structure and Polymorphism

UELI AEBI, WALTER E. FOWLER, GERHARD ISENBERG, THOMAS D. POLLARD, and
P. R. SMITH
Department of Cell Biology and Anatomy, The Johns Hopkins University School of Medicine, Baltimore,
Maryland 21205, and Department of Cell Biology, New York University School of Medicine, New York
10016. Dr. Isenberg's present address is the Max Planck Institute for Psychiatry, D-8000 Munich 40,
Federal Republic of Germany.

ABSTRACT   Crystalline sheets of *Acanthamoeba* actin induced by the trivalent lanthanide gadolinium exist in three different polymorphic forms, which show different striation patterns and surface topographies. We have called these different forms "rectangular" and "square" sheets, and "cylinders" and have shown that each of the three forms is constructed from common "basic" lattices associated in different ways. We have used image processing of electron micrographs to obtain a model for the actin molecule in projection to a resolution of 1.5 nm. The overall dimensions observed in these images are 5.6 X 3.3 X 4.5 nm, and the molecule itself appears distinctly bilobed with the two lobes separated by a cleft. Actin monomers in the sheets are arranged with P2 symmetry and are therefore packed in a manner different from that of the molecules in actin filaments. Because ~35% of the surface area of the actin molecule is exposed on the surface of these sheets, the sheets should be useful to study the stoichiometic binding of actin-binding proteins to the actin molecule.

Actin is a protein that is ubiquitous in nature. It plays a key role in the contractile apparatus of muscle cells and in intracellular processes such as nonmuscle cellular movements. Whereas in muscle cells actin is found exclusively in the form of sedimentable filaments ("thin filaments"), in many nonmuscle cells a significant fraction of the actin seems to exist in a nonsedimentable form (e.g., 3, 7, 18). At low ionic strength, purified muscle and nonmuscle actins are monomeric (G-actin); polymerization into filaments (F-actin) occurs when the ionic strength is raised to physiological levels. In nonmuscle cells, where the ionic strength is relatively constant, the oligomeric state of actin is therefore almost certainly controlled by its interactions with other intracellular proteins (e.g., 9, 11).

To understand the interactions of actin with these regulatory proteins and its role in muscle contraction and cell motility, it is necessary to study actin's molecular structure. Electron microscopy combined with image reconstruction techniques has been used to obtain low-resolution three-dimensional models of F-actin, thin filaments, and decorated thin filaments from muscle (14, 20, 26) and actin filament bundles from nonmuscle cells (5, 19). In all these cases actin filaments have been found to have a discrete helical structure and appear to be constructed from two strands of actin molecules wound around one another. However, disorder in actin filaments visualized after preparation for electron microscopy has limited the obtainable resolution of reconstructions of the actin molecule to ~3 nm, a level at which little molecular substructure can be identified.

The fact that purified actin tends to form filaments under a wide variety of conditions has made it very difficult to obtain three-dimensional crystals suitable for x-ray diffraction analysis at high resolution. Recently, several groups have succeeded in growing crystals of actin complexed 1:1 with protein molecules that block polymerization, i.e., profilin (4) and DNase I (13, 23). A preliminary 0.6-nm map from the actin–DNase I crystals has recently been reported (22). Unfortunately, separation of the map into an actin and a DNase I region is not yet unambiguous at this resolution.

An alternative approach has become feasible with the discovery of thin crystalline sheets of skeletal muscle actin formed in the presence of the trivalent lanthanide, gadolinium (6). Under the conditions originally employed two types of ordered structure were formed, which were described as "tubes" and "microcrystals," together with contaminating filamentous material. Refinements in the preparation technique (2) have allowed the efficient generation of actin sheets, regular to better than 1 nm, that are potentially suitable for high-resolution

study using the tilted-view reconstruction methods introduced by Henderson and Unwin (10).

In this paper we describe the structures of the different polymorphic forms of crystalline *Acanthamoeba* actin sheets induced by gadolinium. We find three distinct types of crystalline structures: "rectangular" sheets, "square" sheets, and "cylinders." Electron micrographs both of negatively stained, and of freeze-dried and heavy-metal-shadowed specimens have been studied by optical diffraction and computer image processing. We have found that all of the different types of sheets are derived from a common "basic" sheet (2). Furthermore, we have obtained a model of the actin molecule in projection to a resolution of 1.5 nm by computer-filtering images of each of the different sheet types. A discussion is presented of the structures of the sheets and their utility in a study whose aim is to understand the structure of actin and its interactions with accessory proteins.

MATERIALS AND METHODS

Materials

All chemicals not otherwise specified were of reagent grade. ATP (sodium salt, grade I) was purchased from Sigma Chemical Co. (St. Louis), PIPES from Calbiochem Behring Corp. (La Jolla, Calif.) and gadolinium trichloride from Aldrich Chemical Co. (Milwaukee, Wisc.).

Proteins

Acanthamoeba actin was purified as a by-product of myosin II (15). After chromatography of the sucrose extract on DEAE-cellulose, fractions enriched in myosin II were pooled, and actomyosin II was precipitated by ATP depletion with hexokinase. The actomyosin II was dissolved in KI and fractionated by gel filtration. Fractions containing purified actin were dialyzed against several changes of 2 mM Tris, 0.5 mM dithiothreitol, 0.2 mM $CaCl_2$, and 0.2 mM ATP to remove KI, and then clarified. Alternatively, the DEAE fractions enriched in actin, which elute at higher KCl concentrations than myosin II, were pooled and the actin was purified according to Gordon et al. (8). *Physarum* actin was a generous gift of Dr. Mark Adelman (Uniformed Services University of the Health Sciences, Bethesda, Md.). Rabbit skeletal muscle actin was prepared from an acetone powder by one cycle of polymerization/depolymerization followed by chromatography on a Sephadex G-150 column (12).

Sheet Preparation

Actin at 0.5–1.5 mg/ml was dialyzed against 2.5 mM imidazole, pH 7.25 (4°C), 0.25 mM dithiothreitol, and 0.005% NaN_3 for 5 h at 4°C. This precrystallization step was used to remove excess ATP from the sample; if omitted, an insoluble complex of ATP and gadolinium will form in the subsequent crystallization step. The dialysis bag (12,000 mol wt exclusion limit, 0.25-inch diameter) was then transferred to 2.5 mM PIPES, pH 7.00 (4°C), 0.25 mM dithiothreitol, and 0.005% NaN_3, containing variable amounts of $GdCl_3$ and KCl ("sheet buffer"). With proper salt and $GdCl_3$ concentrations, sheets will be seen to be forming after ~2.5-h dialysis at 4°C. The rate of dialysis, as well as the amount of KCl and the molar ratio of Gd:actin, are critical variables for crystallization: if dialysis is too fast only random aggregates form, and if dialysis is too slow then filamentous material predominates.

Electron Microscopy

For negative staining, 2.5-μl samples were adsorbed for 60 s to carbon-coated 400 mesh/inch copper grids that were rendered hydrophilic by glow discharge for 15 s in air at low pressure. The grids were washed for 30 s on several drops of distilled water and stained for 30 s on several drops of 0.75% uranyl formate, pH 4.25.

Adsorption freeze-drying and unidirectional Pt-C shadowing were performed on unfixed samples as described by Smith (16); the elevation angle for shadowing was ~30°.

Microscopy was performed on a Zeiss EM 10C electron microscope equipped with a Zeiss Micro-Dose-Focusing unit. All micrographs were taken at a nominal magnification of × 50,000. Magnification was calibrated using catalase crystals (27). For some micrographs, the total electron dose for the specimen (including initial search, focusing, and exposure of film) was kept to <0.05 e⁻/nm² using the

Micro-Dose-Focusing unit and the general approach described by Unwin and Henderson (25); the figure captions indicate such micrographs.

Image Processing

Micrographs were screened by optical diffraction to select those showing the highest resolution. These were scanned directly with a Perkin-Elmer 1010A flatbed scanner (made available through the generosity of Dr. J. Frank of the Division of Laboratories and Research, New York State Department of Health, Albany, N. Y.), using a scanning raster of 13 μm and a spot size of 11 μm, which corresponds to a distance of 0.3 nm on the specimen. The micrographs were carefully aligned so that they were scanned parallel to the *b*-axis of the sheets. The digitized images were displayed, and areas were selected for Fourier transformation that appeared by eye to be regular, uniform in density, and free from dislocations, damage, and dirt. Relatively large areas were transformed (960 × 992 for the rectangular and square sheets, 640 × 475 for the cylinder, and 720 × 700 for the basic sheet) but only rectangular boxes centered near the reciprocal lattice reflections were stored for further processing. The position of each reflection was located by eye on the basis of the position of the amplitude maximum and the constancy of phase over the reflection, and a lattice was refined through the points selected. An array was extracted by bilinear interpolation from the transform at the points on the refined lattice. This array should provide a good representation of the phases of the structure factors but will generally poorly represent their amplitudes: this interpolated array was called the "phase" array. Amplitudes were obtained by integrating the powers over the reflections on the refined lattice, and the "phase" and "amplitude" information was combined to give the final transform.

Common structure factors found in the rectangular and square sheets were deleted and replaced by suitably scaled and phased structure factors obtained from images of basic (for the square type) and square (for the rectangular type) sheets where the appropriate structure factors are uncontaminated. The correct scales and phases were obtained by comparing the total powers of the images after correct translational alignment. Reconstructions made from both uncorrected data and data from which the common spots had been deleted were strongly similar to one another and to the corrected filtrations.

The relative shifts between the upper and lower lattices of the rectangular and square sheets were obtained by measuring the relative translations of filtered unit cells from each of two basic lattices from which the sheets were constructed.

Filtered unit cells from each of the four types of sheet were floated to zero mean and were twofold symmetrized about optimal twofold symmetry centers, incurring no more than a 2.5% loss in the total power in the process. All images were scaled to the same total power and were displayed using contouring and a Photomation P-1700 film writer (Optronics International, Inc., Chelmsford, Mass.), generally following the procedure described by Smith et al. (16) and Aebi et al. (1).

RESULTS

Preparation of Crystalline Sheets of Acanthamoeba Actin

Dialysis at 4°C of purified *Acanthamoeba* G-actin (0.5–1.5 mg/ml) against sheet buffer (see Materials and Methods) containing a 9:1 molar excess of gadolinium (Gd) and 150 mM KCl converts >95% of the soluble G-actin into an insoluble form that can be collected by centrifuging at 5,000 g for 3 min. Examination of this material in the electron microscope shows that it consists of several different types of crystalline sheets (Fig. 1). We have called these (*A*) rectangular sheets and (*B*) square sheets, named for the pattern of striations they show, (*C*) cylinders, which are hollow tubes in solution that have been flattened onto the support film, and (*D*) basic sheets (see also Figs. 2–5). Under these preparation conditions, no significant amount of filamentous material is present. However, at lower Gd:actin ratios, filamentous material contaminates sheet preparation, and below a molar ratio of 4:1 only filaments and random aggregates are present. The optimal actin concentration for sheet formation is between 0.5 and 1.5 mg/ml. When F-actin instead of G-actin is used as starting material, no sheets are formed.

The proportions of the various sheet types in a sample depends on both the KCl and protein concentrations, as shown
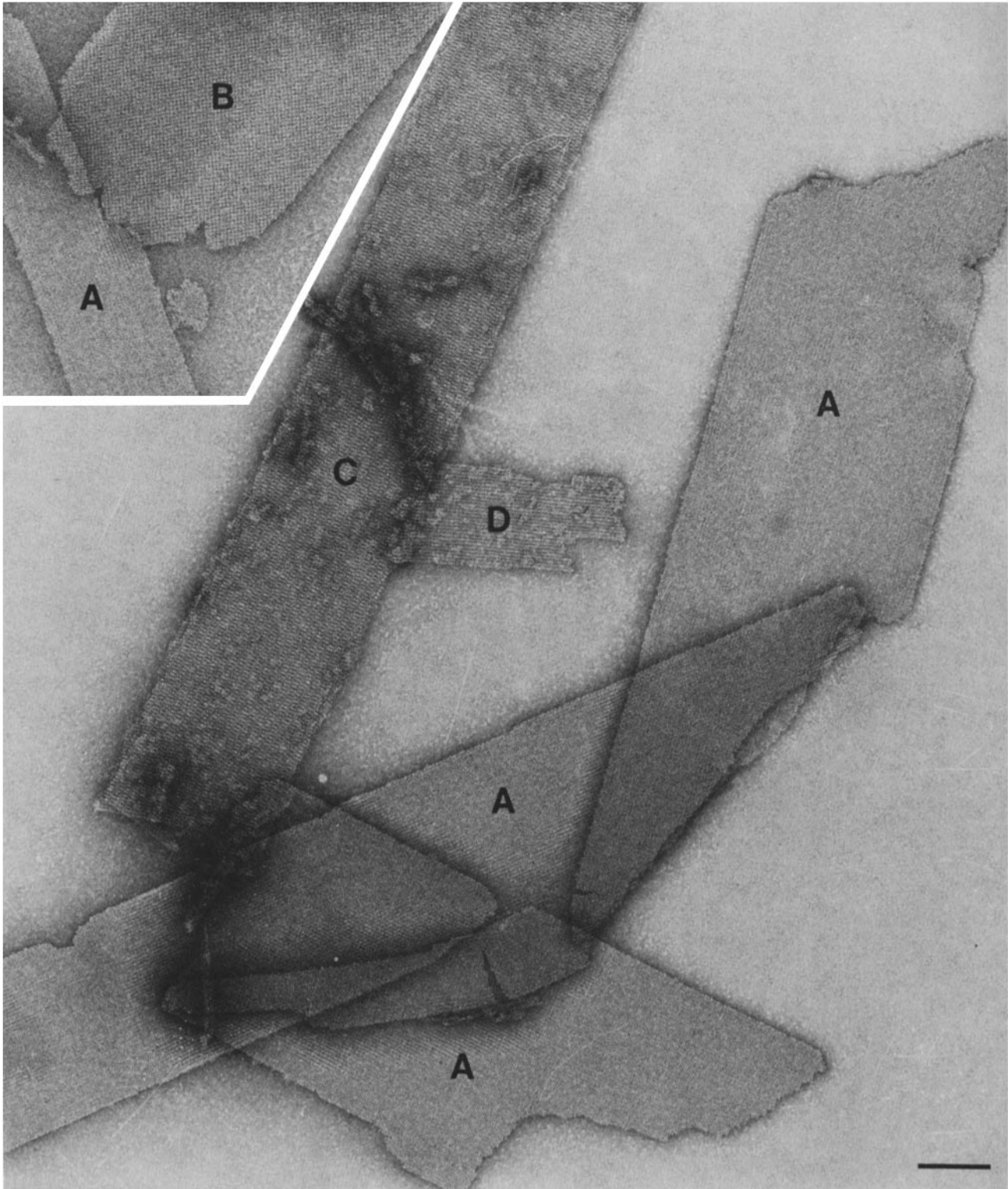
FIGURE 1 Polymorphic forms of negatively stained crystalline actin sheets. (A) Rectangular sheets, (B) square sheet, (C) cylinder, and (D) basic sheet. Bar, 100 nm.

in Table I. The data for each salt concentration come from different sheet preparations because each sheet type, once formed, is fairly stable to changes in salt concentration. A KCl concentration of between 50 and 200 mM is required to produce a significant proportion of sheets; above 225 mM and below 45 mM KCl, no sheets form. At the low salt concentra-

tions (between 50 and 100 mM) rectangular sheets (Fig. 2) predominate. At KCl concentrations between 125 and 175 mM, square sheets (Fig. 3) and cylinders (Fig. 4) are formed, along with some rectangular sheets; square sheets rarely account for >10% of the total. At 200 mM KCl (1 mg/ml protein), cylinders are the main species present. Transitional structures that exhibit

characteristics of both rectangular sheets and cylinders are also seen under conditions favorable to the formation of cylinders (see Table I and Fig. 7 c, *lower panel*).

Stability of Acanthamoeba Actin Sheets

Acanthamoeba actin sheets are stable for weeks in sheet buffer at 4°C as long as the protein concentration is kept above 0.5 mg/ml, but they do aggregate with time. However, when sheet preparations are dialyzed against Gd-free buffer containing KCl, all sheets are converted to filamentous material in <5 h. Sheet preparations at a concentration of >0.5 mg/ml

protein dialyzed against Gd-free, salt-free buffer remain intact for ~24 h, after which they slowly disintegrate. However, if after only 12 h of dialysis against Gd-free, salt-free buffer the sheets are dialyzed against F-actin buffer (2 mM $MgCl_2$, 50 mM KCl), the sheets are completely converted to F-actin.

Attempts were made to convert one type of sheet to another by dialyzing sheets formed at one salt concentration against Gd-containing buffer containing a different concentration of salt. By increasing the salt concentration, a partial conversion of rectangular sheets to cylinders can be effected, but the reverse has not been observed. If sheets are dialyzed for several days against buffer containing gadolinium but not salt, <25%
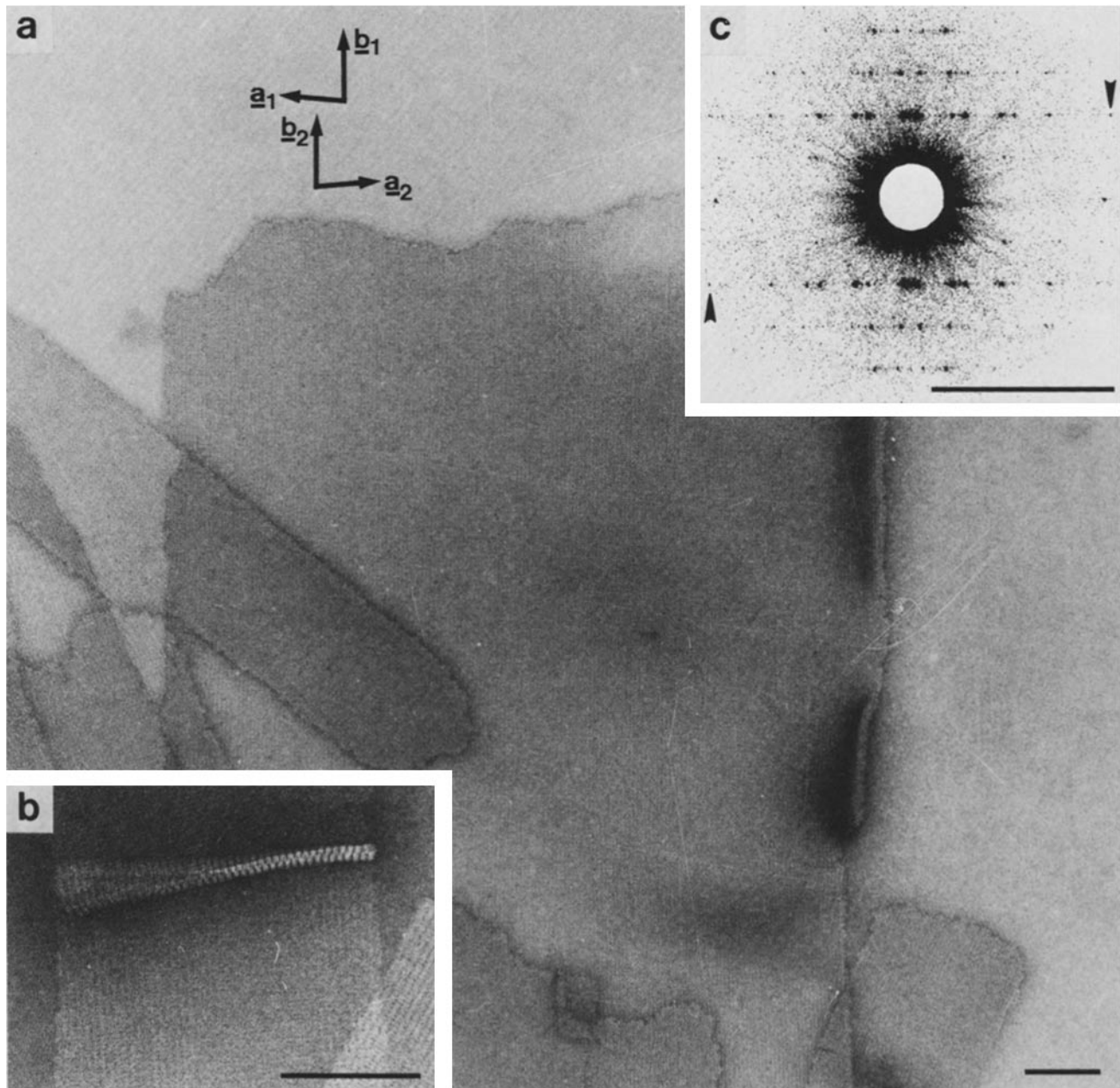

FIGURE 2   (a) An electron micrograph of negatively stained rectangular sheets recorded under minimum dose conditions with an accumulated electron dose of ~0.05 e^-/nm^2. The two pairs of lattice vectors for the two constituent basic lattices are oriented with respect to the large rectangular sheet. (b) A fold in a rectangular sheet showing its two layers and their relative stagger along the a axis. (c) This diffraction pattern was recorded from a circular area of a sheet ~350 nm in diameter; the arrowheads point to a Friedel pair of reciprocal lattice reflections corresponding to 1.2 nm resolution. Extra diffraction spots can be seen because the diffracted area included a dislocation zone. These zones can be seen by viewing micrographs of rectangular sheets at a glancing angle from the side (along the a lattice vectors). Bars, 100 nm (a and b) and 1.5 nm^{-1} (c).
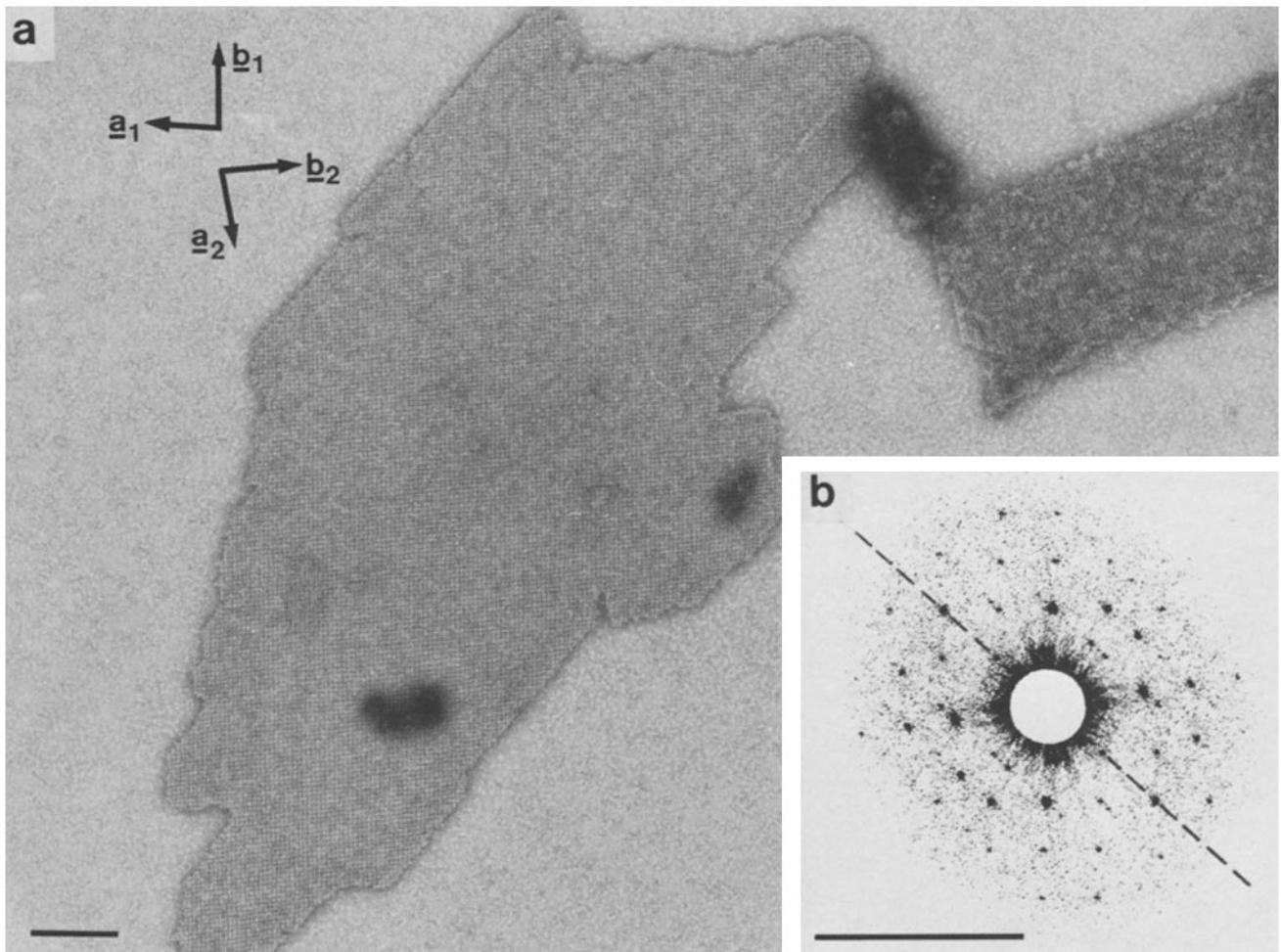
FIGURE 3 An electron micrograph and optical diffraction pattern of a negatively stained square sheet. (a) Micrograph with two pairs of basic lattice vectors oriented with respect to the square sheet. (b) This diffraction pattern was recorded from a circular area of the sheet ~250 nm in diameter. Bars, 100 nm (a) and 1.5 nm^{-1} (b).

of the higher-order sheets are converted into pieces of basic sheet (see also reference 2). These experiments are summarized in Table II.

The Basic Sheet

The basic sheet is found in some *Acanthamoeba* actin sheet preparations, and its unit cell morphology in projection has been determined for negatively stained basic sheets (2). Conditions, such as protein concentration and ionic strength, can be adjusted to favor the conversion of higher-order sheets to basic sheets (see above and Table II; also reference 2), but basic sheets never account for >25% of the crystalline material present. Some of the features of the basic sheet are indicated in Fig. 5: it is constructed on a near-rectangular lattice with average unit cell parameters $a = 5.65$ nm, $b = 6.55$ nm, and $\gamma = 85.5°$. A striking feature of the basic sheet is the difference in the topographies of its two surfaces visualized on freeze-dried and shadowed specimens (Fig. 5c): one surface of the basic sheet appears coarse and untextured with no apparent lattice, and the other appears smooth and textured with the same near-rectangular lattice as the negatively stained basic sheet. While negatively-stained basic sheets are found with both right-handed and left-handed lattices (depending on their orientation on the microscope grid), the lattice on the textured

surface of a freeze-dried and shadowed basic sheet is always right-handed (Fig. 5c). The shadow lengths in this type of preparation indicate that the basic sheet is ~4.5 nm thick. The 1.5-nm resolution filtration of the negatively stained basic sheet in projection (2) shows that there are two bilobed actin monomers per unit cell related by a twofold axis of symmetry normal to the sheet plane (space group P2). Because the two surfaces of the basic sheet are clearly different, the actin monomers must be asymmetric in the direction normal to the sheet plane, and all the molecules in a basic sheet must be oriented with the same polarity in this direction.

Morphology and Lattice Parameters of Higher-Order Sheets

Rectangular sheets (see Figs. 1 and 2) can grow to several microns in length and up to 1 μm in width; they exhibit characteristic transverse and longitudinal striations that have different separations (6.5 nm and 5.6 nm, respectively). Square sheets (see Figs. 1 and 3) can grow to over 0.5 μm in width but do not have a characteristic overall shape. They have two families of near-orthogonally related striations that have the same separation (5.6 nm) and usually extend diagonally from the sheet edges. Cylinders (see Figs. 1 and 4) have a flattened width of 225 nm, length of up to 5 μm, and two families of

diagonal striations with the same separation (5.6 nm) with pitches of ±11.9°.

Freeze-dried and shadowed specimens (Fig. 6) provide information about the thickness and the surface topography of the higher-order sheets. Shadow lengths give a value of ~9 nm for the thickness of rectangular and square sheets, which is consistent with a thickness of two actin molecules (see also Fig. 2 b). Both the rectantangular and the square sheets in this type of preparation (Figs. 6 a and b) have two textured surfaces with identical right-handed near-rectangular lattices ($a = 5.50$ nm, $b = 6.35$ nm, $\gamma = 86.5°$), whereas cylinders (Fig. 6 c) have a coarse surface structure with no apparent lattice. Fractured ends of cylinders allow their inner surfaces to be seen, which clearly show a surface topography indistinguishable from that of rectangular and square sheets. These observations suggest that all three higher-order sheets are constructed from basic sheets.

This interpretation is supported by the existence of transition structures that show both basic sheet and higher-order sheet regions. Fig. 7 shows examples of transitions between each of the three higher-order sheet types and basic sheets. These examples demonstrate unambiguously the continuity of the basic sheet with the other sheet types and establish the orienta-

tion of the constituent basic sheet lattices with respect to the structure of the higher-order sheets.

The overall construction scheme of the three higher-order sheet types can be seen best by indexing optical diffraction patterns of micrographs of each sheet type with respect to the underlying basic sheet lattice. All of the diffraction maxima from the three different types of higher-order sheets can be indexed on one of two such basic lattices (Fig. 8) as the data collected in Table III indicate.

In the rectangular sheets, two basic lattices are associated in an apolar fashion with their b vectors parallel. Since both sides of the sheets show a regular surface structure, the coarse sides of the two constituent basic sheets must be in contact (see Fig. 2 b). In the case of the square sheet, two basic lattices again associate in an apolar fashion, but the two b vectors are rotated by 85° with respect to each other. Finally, the cylinders can be explained by folding the basic lattice into a cylindrical shell with the lattice lines having an average pitch of 12° and with the coarse surface of the basic sheet forming the outer surface of the cylinder.

We have attempted to index the rectangular and square sheets on superlattices containing actin monomers in both the basic sheets from which they are made. Although it is easy to
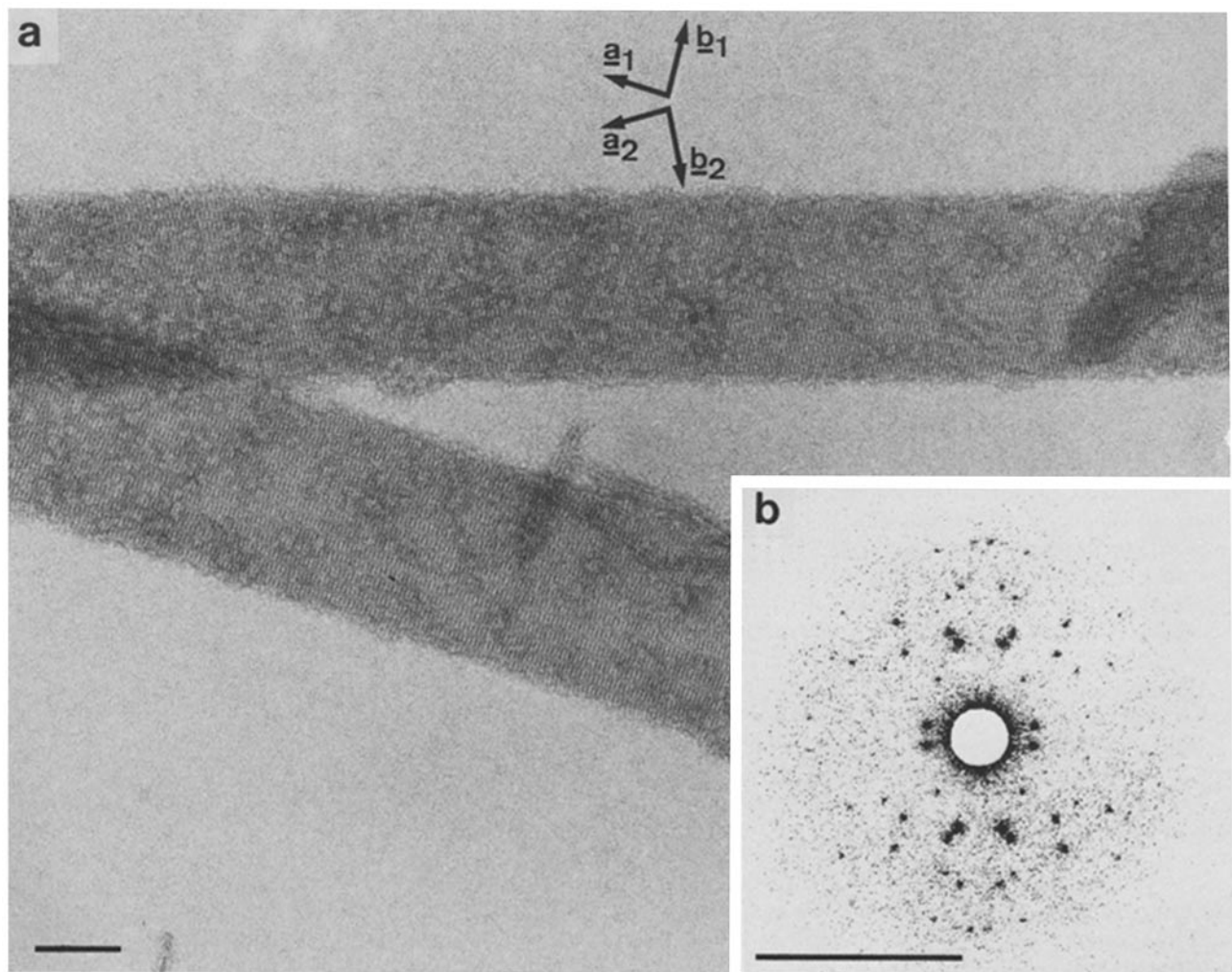

FIGURE 4   An electron micrograph and optical diffraction pattern of negatively stained cylinders. (a) This micrograph was recorded under minimal dose conditions with an accumulated electron dose of ~0.05 e⁻/nm². The two pairs of basic lattice vectors are oriented with respect to the upper cylinder. (b) This diffraction pattern was recorded from a circular area on the upper cylinder ~200 nm in diameter. Bars, 100 nm (a) and 1.5 nm⁻¹ (b).
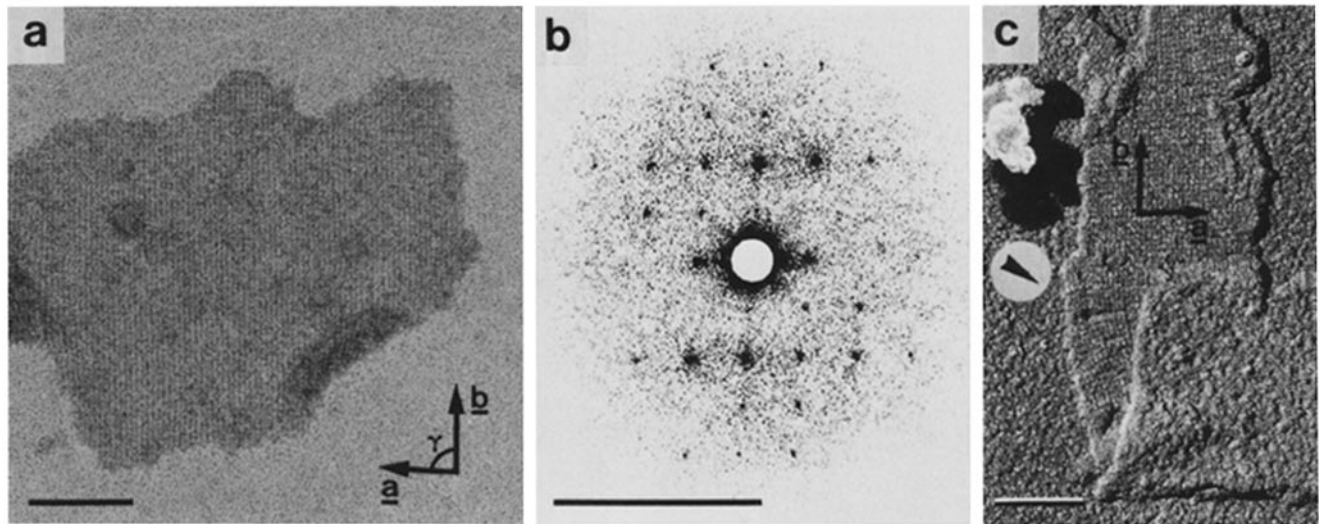
FIGURE 5 The basic sheet. (a) Electron micrograph of negatively stained basic sheet with lattice vectors oriented to the sheet. (b) Optical diffraction pattern of the micrograph in a recorded from a circular area ~200 nm in diameter. (c) A freeze-dried and shadowed piece of basic sheet that has folded over onto itself to show a "textured" surface with a regular lattice, and a "coarse" surface with no visible lattice. Arrowhead indicates the direction of shadowing. Bars, 100 nm (a and c) and 1.5 nm^{-1} (b).

TABLE I

Proportions of Sheet Types

Protein concentration	KCl	Rectangular	Square	Cylinders	Transitional
mg/ml	mM	%	%	%	%
1.0 (1.5)	75	100 (100)	0 (0)	0 (0)	0 (0)
1.0 (1.5)	100	80 (100)	0 (0)	0 (0)	20 (0)
1.0 (1.5)	125	60 (85)	5 (5)	10 (0)	25 (10)
1.0 (1.5)	150	40 (70)	10 (10)	20 (5)	30 (15)
1.0 (1.5)	175	20 (50)	5 (5)	50 (15)	25 (30)
1.0 (1.5)	200	0 (25)	0 (0)	90 (50)	10 (25)

Buffer used: sheet buffer with 9:1 molar excess of GdCl$_3$ to actin and KCl concentrations as indicated. Under these conditions >90% of the aggregated material appears in the form of sheets as judged by electron microscopy. Transitional structures are defined as sheets that exhibit characteristics of both rectangular sheets and cylinders (see Fig. 7 c, lower panel).

TABLE II

Results of Actin-sheet Dialysis

Sheet buffer*	Time scale	Result
Gd, KCl	Weeks	Slow aggregation
Gd, no KCl	Days	Some conversion of higher-order sheets to basic sheet pieces (≤25%)
no Gd, KCl	Hours	Complete conversion to filamentous material
no Gd, no KCl	Days	Disintegration
no Gd, no KCl (12 h), followed by 50 mM KCl, 2 mM MgCl$_2$	Hours	F-actin
Gd, increased KCl (100 → 175 mM)	Days	Partial conversion of rectangular sheets to cylinders
Gd, decreased KCl (175 → 100 mM)	Days	No change

* Actin sheets (1 mg/ml) were dialyzed at 4°C against sheet buffer containing the indicated substances.

locate one of these putative lattice vectors in each case (5.57 nm perpendicular to b for the rectangular sheet, and 8.47 nm along the long diagonal in the square sheet), we are unable to define the corresponding lattice vectors that should be perpendicular to them. If they exist, they must be longer than 200 nm, the highest resolution of our indexation measurements. The consequence of this situation is that the contacts formed between the coarse surfaces of the basic sheets that make up a higher-order sheet are rather heterogeneous. This may explain why they split relatively easily into their component basic sheets under appropriate ionic conditions.

The rectangular sheets depart from complete regularity in that dislocation zones may be found as strips along their length. Within these strips, one of the two lattices is sheared with respect to the corresponding lattices in the neighboring zones while being continuous with them at the edge of the zone. Although each zone is of constant width along its length, different zones may have widths from 100 to several hundred nanometers. An optical diffraction pattern from an area that overlaps two or more zones will show extra spots on the $k = n$ lattice lines that have come from the different sheared lattices. Such spots can be seen in Fig. 2 b, where a large area was taken

for optical diffraction: areas used for computer filtration were smaller and were confined to a single zone.

Unit-cell Morphology of the Different Types of Sheets

Filtered images were obtained from basic sheets and from both sides of each of the higher-order actin sheets. The two sides could be completely separated in the case of the cylinders, but this could not be done for the rectangular and square sheets because the diffraction patterns show "common" spots (e.g., the equator in the rectangular sheets [Fig. 2 c], and a diagonal indicated by a dotted line in the case of the square sheets [Fig. 3 b]). Single-sided filtrations for rectangular and square sheets were obtained by supplying complementary information to replace the contaminated structure factors, as described in Materials and Methods. The filtered images were contoured as shown in Fig. 9. For the higher-order sheets, filtrations of both constituent basic sheets (i.e., "top" and "bottom") were virtually identical (data not shown).

A comparison of filtered unit cells from the top and bottom lattices of the same rectangular and square sheets allows one to determine the relative stagger of the two lattices in each of the two sheet types. For the rectangular sheets the stagger was found to be exactly one half unit cell perpendicular to b. This is qualitatively confirmed by examination of occasional "folds" found in rectangular sheets, as illustrated in Fig. 2 b. In the case of the square sheets, the shorter of the two diagonals in the unit cells in the upper and lower basic sheets lay over one another: this diagonal is indicated by a dotted line in Fig. 9 b.

The unit cell in all the filtrations contains two actin monomers related by a twofold axis of symmetry perpendicular to the sheet plane, as reported previously for the basic sheet (2). Each actin monomer is an asymmetric, elongated, globular molecule with apparent overall dimensions of 5.6 × 3.3 × 4.5 nm. The head-to-tail connectivity of monomers along the a-axis is clearly delineated in the filtrations from all sheet types.

The filtrations from cylinders and basic sheet reveal elongated actin monomers in about the same orientation with respect of the near-rectangular lattice as those in rectangular and square sheets. However, the stain distributions in these two differ somewhat from that of the rectangular and square sheets. The principal reason for this difference is that the images of the rectangular and square sheets contain higher resolution information than the images of the basic sheets and cylinders. This has tended to sharpen the edges of the stain regions in the images in Fig. 9 a and b relative to those in Fig. 9 c and d. This is supported by the observation that limiting the resolution of the images to 2 nm smooths the edges of the images in Fig. 9 a and b, while leaving those of Fig. 9 c and d largely unaffected (data not shown).

A second cause of the observed differences may arise because the coarse surfaces of rectangular and square sheets are in close association and are therefore relatively inaccessible to stain.
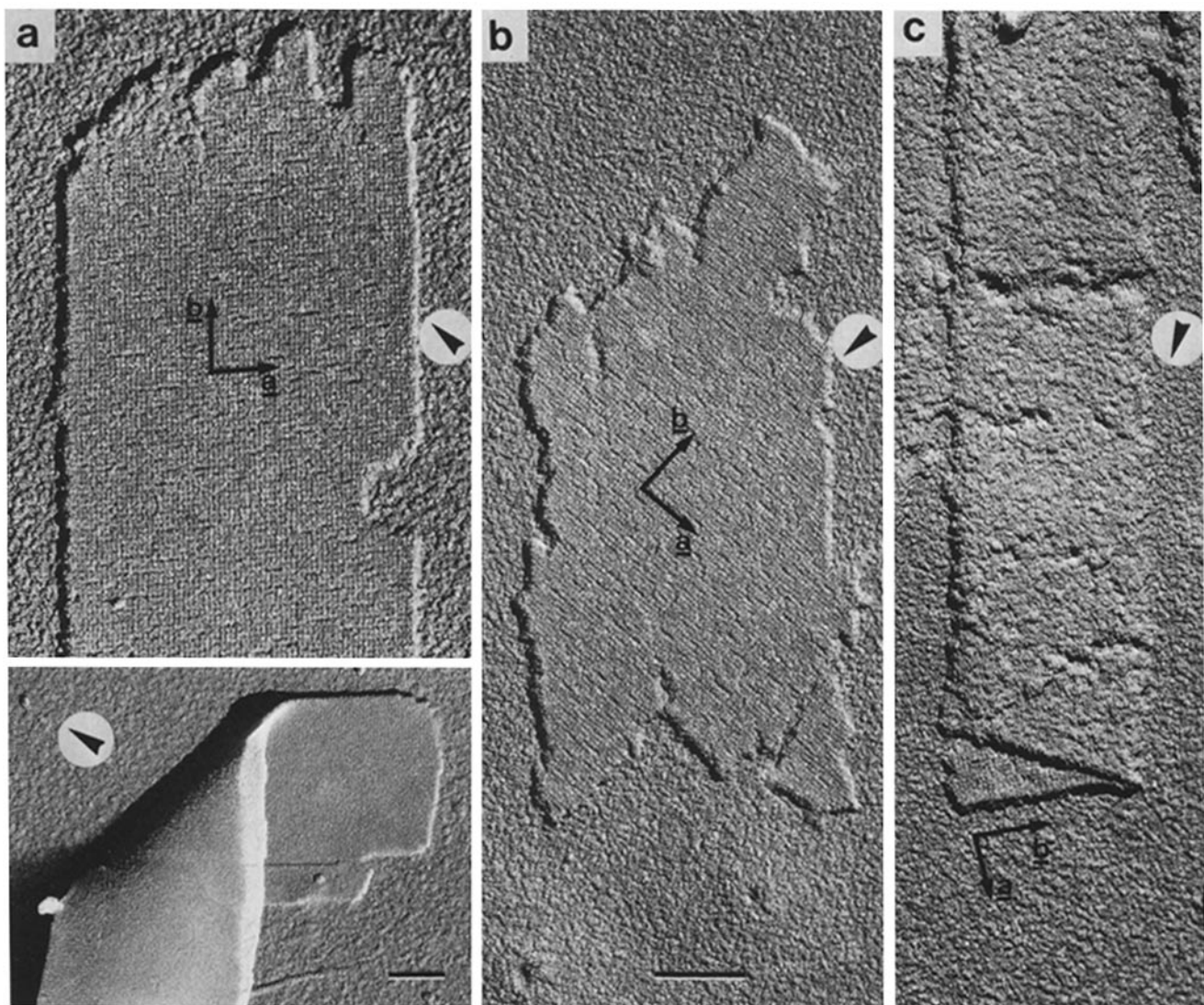

FIGURE 6 Freeze-dried and shadowed higher-order sheets. (a) Electron micrographs of rectangular sheets; the folded rectangular sheet in the lower panel shows the lattice characteristic of the regular surface of the basic sheet on both its surfaces. (b) Electron micrograph of square sheet with the same surface lattice exhibited by the rectangular sheet. In this case, however, the lattice vectors extend diagonally from the sheet edges, which is characteristic for square sheets (see Figs. 1 and 3). (c) Electron micrograph of cylinder. Note the irregular surface characteristic of the coarse surface of the basic sheet. At the end of the cylinder, however, the exposed inner surface exhibits a lattice identical to that found on the surfaces of rectangular and square sheets and the regular side of the basic sheet. The basic lattice vectors are indicated in $a-c$. Arrowheads indicate direction of shadowing. Bars, 100 nm.
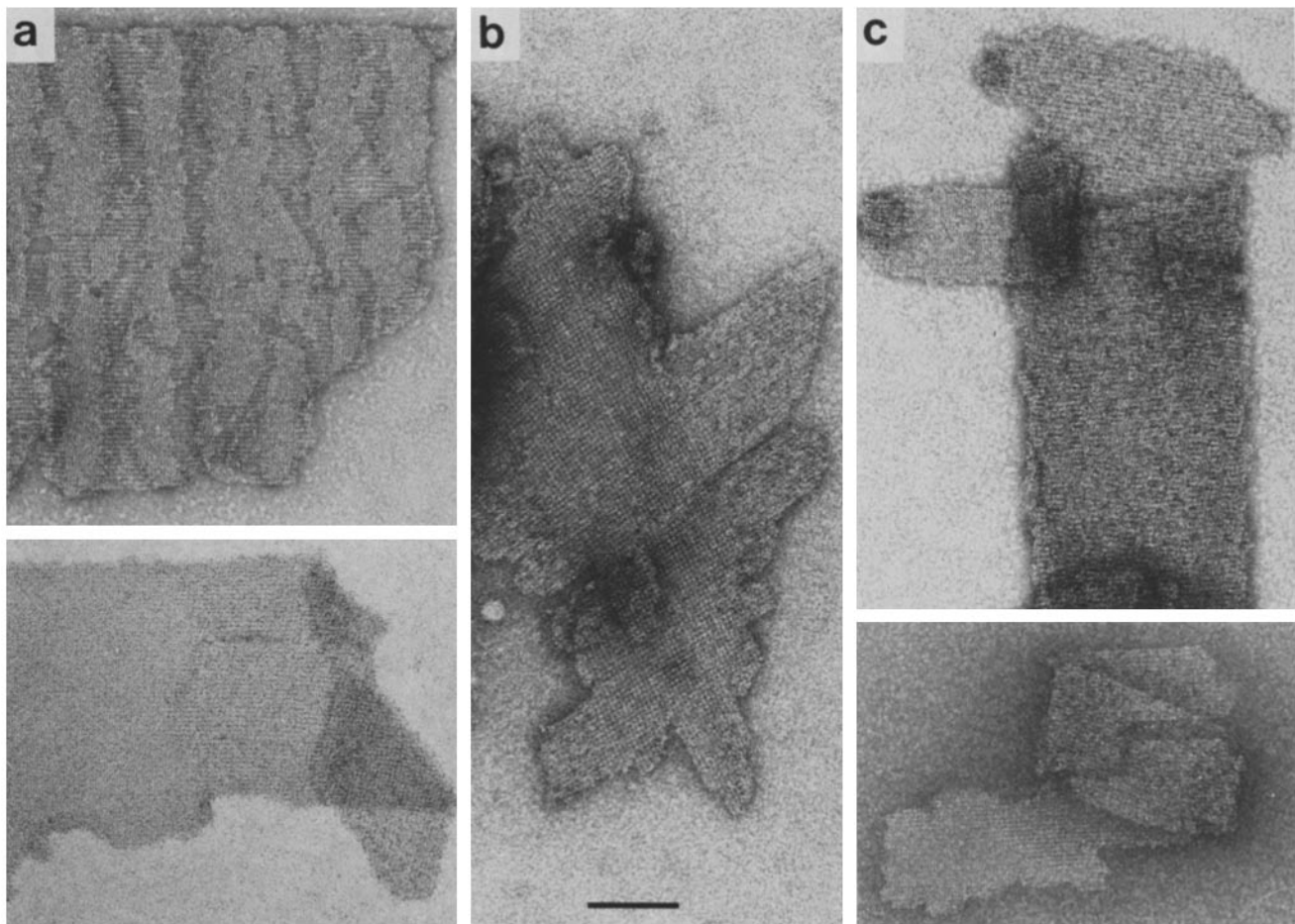
FIGURE 7 Electron micrographs of negatively stained transition structures. (a) Examples of sheets that include both rectangular sheets and basic sheet regions. (b) An example of a sheet that includes both square sheet and basic sheet regions. (c) Examples of sheets that include both cylinder and basic sheet regions; the example in the lower panel also includes a piece of rectangular sheet. Bar, 100 nm.

The cylinders and basic sheets, on the other hand, have both their textured and coarse surfaces freely accessible to stain, which may allow additional features of the actin monomers to be mapped out. It should be possible to determine whether such effects are important by looking at unstained specimens, an approach we are currently investigating.

Certain high-resolution features (e.g., the "double arms" connecting the two molecules in the dimer) are present only in the reconstruction obtained from the rectangular sheet (see Fig. 9 a). This is not surprising, because this type is the largest and the best preserved in negative stain. In fact, in a few cases we have recorded reflections out to 1.0 nm^{-1} in optical diffraction patterns from low-dose images (data not shown). We have therefore chosen the rectangular sheet for use in a high-resolution structural analysis of the actin molecule, as discussed below.

Sheets Formed from Different Actins

Gadolinium induces sheet formation in actins prepared from several different sources. We have made rectangular sheets and cylinders from skeletal muscle actin, which are analogous to the "microcrystals" and "tubes" made from skeletal muscle actin by dos Remedios and Dickens (6). However, our preparations contain a higher percentage of crystalline material and much larger rectangular sheets than reported by these authors.

We have never observed production of rectangular sheets in the absence of salt, as reported by dos Remedios and Dickens (6), but the salt requirement for skeletal muscle is much lower than that of Acanthamoeba actin. We have also made sheets from Physarum actin and from chicken gizzard (smooth muscle) actin, and sheets have also been obtained from Dictyostelium actin (J. Spudich, personal communication). The major difference in the conditions for sheet formation for these different actins is in the requirement for a specific ionic strength, but the dependence of sheet formation on the gadolinium to actin molar ratio is similar for all the different actins. Square sheets have only been observed with Acanthamoeba actin; however, the same wide range of conditions used for sheet formation in the case of Acanthamoeba actin has not yet been explored with any of the other actins.

DISCUSSION

We have described conditions for the production of large crystalline sheets from Acanthamoeba actin and have shown that the polymorphic crystal forms observed are all related by a common basic lattice. Freeze-dried and shadowed specimens reveal the surface topographies of the different forms that define the polarity of the two basic sheets making up each type. The upper part of Fig. 10 summarizes the relationship between the basic lattices in each of the different sheet types; the lower

part of Fig. 10 contains diagrammatic end-on views of the sheets that show the polarity of the constituent basic sheets in the direction perpendicular to the lattice plane. For the rectangular and square sheets, Fig. 10 shows the relative stagger of the two basic lattices.

Structural analysis of these actin sheets provides the highest resolution view of the negatively stained actin monomer yet available (~1.5 nm). The actin monomer in projection measures 5.6 × 3.3 nm and is distinctly bilobed; the thickness, as determined from measurements of shadowed speciments and folds in negatively stained sheets, is ~4.5 nm. These dimensions are consistent with those obtained from three-dimensional reconstruction of actin filaments (14).

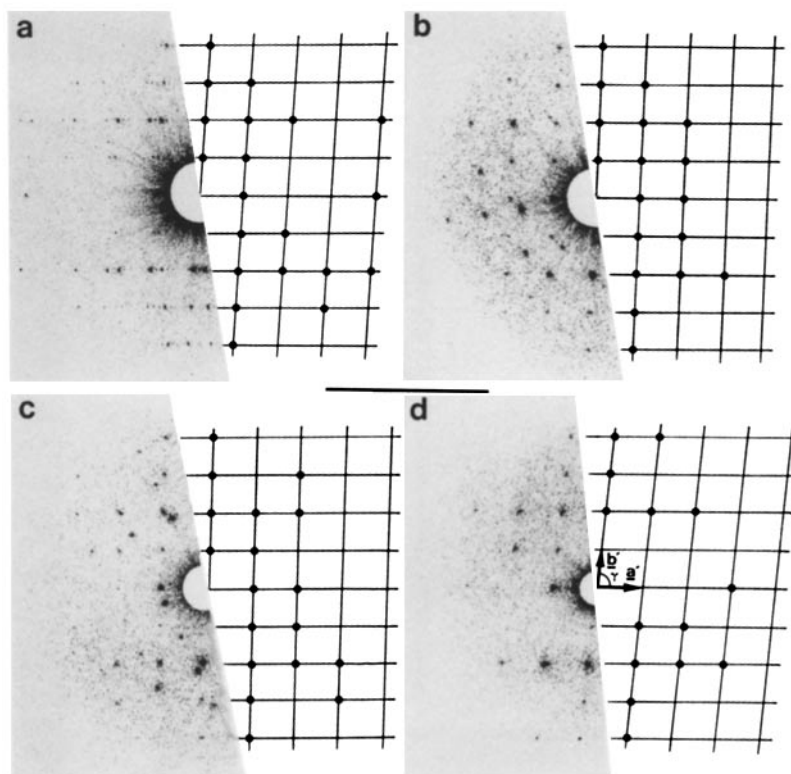The use of minimum-dose techniques in recording micro-

FIGURE 8   Optical diffraction patterns and indexation of one of the two basic reciprocal lattices making up each different type of higher-order sheet. (a) Rectangular sheet. (b) Square sheet. (c) Cylinder. (d) Basic sheet. In d, the reciprocal lattice vectors are indicated. Bars, 1.5 nm^{-1}.

TABLE III

Collected Data

Sheet type	Preparation	Lattice	Measured	a	b	γ^*	ϕ^*	Average diameter or flattened width
				nm	nm			nm
Rectangular	Negative stain	Bottom	56	5.58 ± 0.05	6.57 ± 0.08	82.6 ± 0.8	0.00	100–1,000
	Negative stain	Top	56	5.58 ± 0.06	6.56 ± 0.07	86.1 ± 0.9		
	Freeze-dried & shadowed	Top	18	5.55 ± 0.20	6.40 ± 0.15	86.1 ± 0.8		—
Square	Negative stain	Bottom	34	5.64 ± 0.05	6.50 ± 0.07	86.9 ± 0.7	84.8 ± 0.8	100–750
	Negative stain	Top	34	5.62 ± 0.06	6.52 ± 0.07	87.2 ± 0.7		
	Freeze-dried & shadowed	Top	15	5.50 ± 0.22	6.32 ± 0.19	87.0 ± 1.1		—
Cylindrical	Negative stain	Bottom	36	5.61 ± 0.05	6.40 ± 0.08	85.6 ± 0.9	23.8 ± 1.8	225 ± 5
	Negative stain	Top	36	5.64 ± 0.06	6.51 ± 0.07	85.3 ± 0.8		
Basic	Negative stain	—	60	5.65 ± 0.06	6.55 ± 0.08	85.7 ± 0.8	—	100–500
	Freeze-dried & shadowed	—	28	5.50 ± 0.17	6.35 ± 0.20	86.2 ± 0.6		

Values are given as means with their standard deviations. Bottom (top) lattice: sheet lattice "in contact with" ("pointing away from") the carbon support film. γ, Angle between basic lattice vectors a and b (≤90°); ϕ, angle between b_{bottom} and b_{top}.
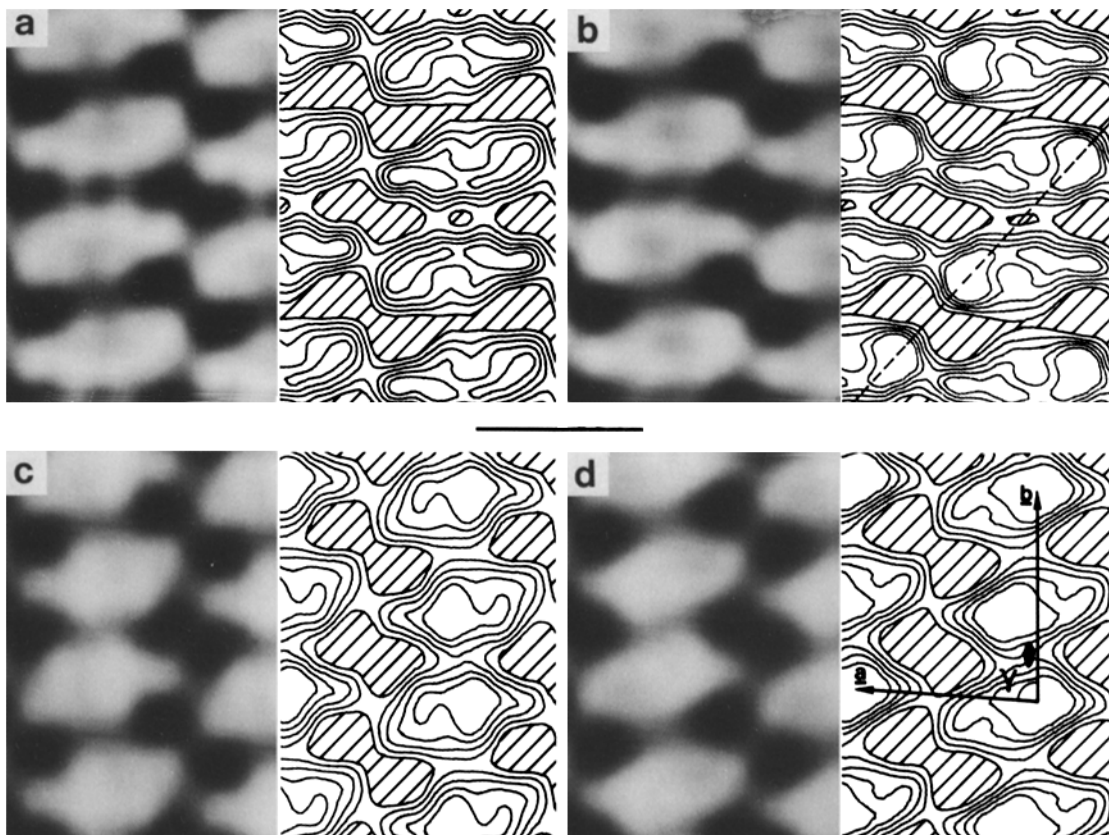* In degrees.

FIGURE 9 Contour maps from computer filtrations of the different types of sheet are shown on the right-hand sides of each panel, with photowritten representations of them on the left. (a) Rectangular sheet. (b) Square sheet: the dotted line shows the diagonal that is superimposed on a similar diagonal in the other basic sheet. (c) Cylinder. (d) Basic sheet. The regions of highest density, which correspond to "holes" filled with negative stain, have been shaded in the contour plots. The actin dimer consists of the pair of monomers adjacent to the crystallographic "twofold" symbol shown in (d). a–c are "single-sided" filtrations; filtrations from the other sides of these higher-order sheets reveal virtually identical structural features. Bar, 5 nm.
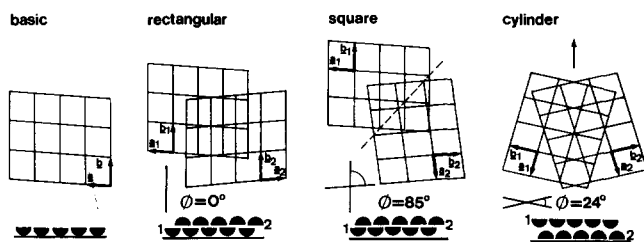

FIGURE 10 Schematic representation of the orientation of the two basic sheet lattices constituting each of the higher-order sheets. The upper diagrams (views perpendicular to the sheet plane) show the relative rotations between lattice vectors b_1 and b_2, and the polarities, indicated by the handedness, of the two basic sheets constituting each of the three higher-order sheets. The relative stagger of the two basic sheet lattices is shown for the rectangular and square sheets. The lower diagrams (end-on views) show the polarities of the basic sheets perpendicular to the sheet plane in each of the three cases; the solid line represents the specimen support film.

graphs of negatively stained specimens is essential in preserving high-resolution detail in the sheets. Using a maximum dose of 0.05 e$^-$/nm^2, we have been able to recover 1.0-nm resolution information from negatively stained rectangular sheets. We are currently collecting data from such preparations for use in a three-dimensional reconstruction of the actin monomer (Fowler et al., manuscript in preparation).

In both actin filaments and actin sheets, there are two rows of actin monomers associated head-to-tail with the same polarity along the row axis. In the filament, the two strands also have the same relative polarity with respect to the filament (or row) axis, but the monomers in each strand have different polarities in the direction normal to the filament axis. This symmetry is seen most easily in the "unwound" filament diagrammed in Fig. 11. In contrast, adjacent rows of monomers in a basic sheet have opposite polarity with respect to the row axis, and the monomers in each strand have the same polarity in the direction normal to this axis (i.e., to the plane of the sheet). The diagrams in Fig. 11 show that sheets cannot be built by a combination of "unwinding" and lateral association of filaments, although it is possible that the head-to-tail contacts within a row or strand are similar in the sheet and the filament.

From considerations of the dimensions of the actin monomer in the sheets and of the characteristic 5.5-nm repeat of monomers along the axis of the actin filament it appears reasonable that the sheet monomer is oriented within the filament with its long axis (i.e., along a) roughly parallel to the filament axis. However, more detailed orientation of the sheet monomer within the actin filament is not yet possible, because of the lack of three-dimensional data about the actin monomer and because of the uncertainty about the position and shape of actin monomers in the actin filament, even given the recent work of Taylor and Amos (24). Improvements in actin filament recon-
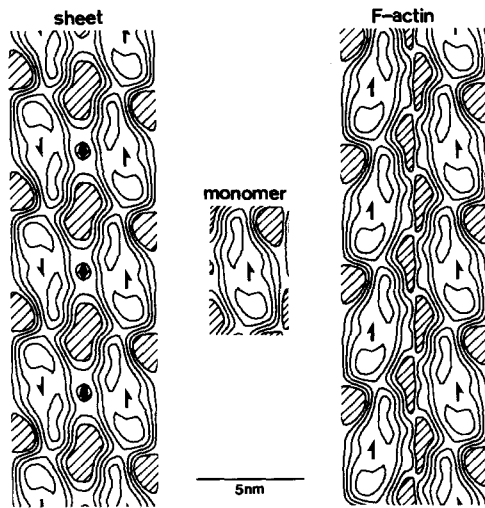
FIGURE 11 A comparison of the quarternary structure of the actin monomer in projection in the basic sheet and the "unwound" actin filament. While the exact orientation of the actin monomer within the filament is tentative, the polarity and stagger of the two "unwound" strands relative to each other are drawn correctly. The contour map of the monomer was obtained from the average of the filtrations of the rectangular and square sheets shown in Fig. 9a and b. The half-arrows indicate the polarity of the actin monomer along the a-axis in the sheet (see Fig. 9d) and the filament axis in the unwound filament, respectively; twofold axes of symmetry are indicated (●). The "holes" filled with negative stain have been shaded.

structions might allow the relative orientation of actin monomers in the sheet and in the filament to be established.

In preliminary experiments we have attempted to label actin sheets using myosin subfragment 1 (S1). We found, however, that S1 caused actin sheets to disintegrate, indicating that the bonds formed between the actin monomers and this actin-interacting protein are stronger than and incompatible with the crystal bonds. That S1 is able to recognize the actin monomers in the sheets and induce the formation of filaments demonstrates that, by these criteria, actin in the presence of gadolinium is still functional.

The polymorphism of actin sheets allows many more binding sites to be potentially available for labeling studies with other actin-binding proteins: both the coarse and the textured surfaces are accessible in the basic sheet and the cylinder, or a minimum of 35% of the surface of the actin monomer. Given the large number of actin-interacting proteins, we are confident that several different binding sites will be localized by studying labeled actin sheets.

We thank Drs. K. A. Taylor and L. A. Amos for giving us a preprint of reference 24.

REFERENCES

1. Aebi, U., R. K. L. Bijlenga, B. ten Heggeler, J. Kistler, A. C. Steven, and P. R. Smith. 1976. Comparison of the structural and chemical composition of giant T-even phage heads. *J. Supramol. Struct.* 5:475–495.
2. Aebi, U., P. R. Smith, G. Isenberg, and T. D. Pollard. 1980. Structure of crystalline actin sheets. *Nature (Lond.).* 288:296–298.
3. Bray, D., and C. Thomas. 1976. Unpolymerized actin in fibroblasts and brain. *J. Mol. Biol.* 105:527–544.
4. Carlsson, L., L.-E. Nystrom, U. Lindberg, K. K. Kannan, H. Cid-Dresdner, and S. Lovgren. 1976. Crystallization of a non-muscle actin. *J. Mol. Biol.* 105:353–366.
5. DeRosier, D., E. Mandelkow, A. Silliman, L. Tilney, and R. Kane. 1977. Structure of actin-containing filaments from two types of non-muscle cells. *J. Mol. Biol.* 113:679–695.
6. Dos Remedios, C. G., and M. J. Dickens. 1978. Actin microcrystals and tubes formed in the presence of gadolinium ions. *Nature (Lond.).* 276:731–733.
7. Gordon, D., J. L. Boyer, and E. D. Korn. 1977. Comparative biochemistry of non-muscle actins. *J. Biol. Chem.* 252:8300–8309.
8. Gordon, D. J., E. Eisenberg, and E. D. Korn. 1976. Characterization of cytoplasmic actin isolated from *Acanthamoeba castellanii* by a new method. *J. Biol. Chem.* 251:4778–4786.
9. Grumet, M., and S. Lin. 1980. A platelet inhibitor with cytochalasin-like activity against actin polymerisation *in vitro. Cell.* 21:439–444.
10. Henderson, R., and P. N. T. Unwin. 1975. Three-dimensional model of the purple membrane obtained by electron microscopy. *Nature (Lond.).* 257:28–32.
11. Isenberg, G., U. Aebi, and T. D. Pollard. 1980. A novel actin binding protein from *Acanthamoeba* which regulates actin filament polymerization and interaction. *Nature (Lond.).* 288:455–459.
12. MacLean-Fletcher, S., and T. D. Pollard. 1980. Identification of a factor in conventional muscle actin preparation which inhibits actin filament self-association. *Biochem. Biophys. Res. Commun.* 96:18.
13. Mannherz, H. G., W. Kabsch, and R. Leberman. 1977. Crystals of skeletal muscle actin: pancreatic DNAase I complex. *FEBS (Fed. Eur. Biochem. Soc.) Lett.* 73:141–143.
14. Moore, P., H. Huxley, and D. DeRosier. 1970. Three-dimensional reconstruction of F-actin, thin filaments and decorated thin filaments. *J. Mol. Biol.* 50:279–295.
15. Pollard, T. D., W. F. Stafford III, and M. E. Porter. 1978. Characterization of a second myosin from *Acanthamoeba castellanii. J. Biol. Chem.* 253:4798–4808.
16. Smith, P. R. 1980. Freeze drying specimens for electron microscopy. *J. Ultrastruct. Res.* 72:380–384.
17. Smith, P. R., U. Aebi, R. Josephs, and M. Kessel. 1976. Studies on the structure of the T4 bacteriophage tail sheath. I. The recovery of three-dimensional structural information from the extended sheath. *J. Mol. Biol.* 106:243–275.
18. Southwick, F. S., and T. P. Stossel. 1981. Isolation of an inhibitor of actin polymerization from human polymorphonuclear leukocytes. *J. Biol. Chem.* 256:3030–3036.
19. Spudich, J. A., and L. A. Amos. 1979. Structure of actin filament bundles from microvilli of sea urchin eggs. *J. Mol. Biol.* 129:319–331.
20. Spudich, J. A., H. E. Huxley, and J. T. Finch. 1972. Regulation of skeletal muscle contraction. II. Structural studies of the interaction of the tropomyosin-troponin complex with actin. *J. Mol. Biol.* 72:619–632.
21. Spudich, J., and S. Watt. 1971. The regulation of rabbit skeletal muscle contraction. I. Biochemical studies of the interaction of the tropomyosin-troponin complex with actin and the proteolytic fragments of myosin. *J. Biol. Chem.* 246:4866–4871.
22. Suck, D., W. Kabsch, and H. G. Mannherz. 1981. The three-dimensional structure of the skeletal muscle-bovine pancreatic DNase I complex at 6 angstroms. *Proc. Natl. Acad. Sci. U. S. A.* 78:4319–4323.
23. Sugino, H., N. Sakabe, K. Sakabe, S. Hatano, F. Oosawa, T. Micawa, and S. Ebashi. 1979. Crystallization and preliminary crystallographic data of chicken gizzard G-actin-DNase I complex and *Physarum* G-actin-DNase I complex. *J. Biochem.* 86:257–260.
24. Taylor, K., and L. Amos. 1981. A new model for the geometry of the binding of myosin crossbridges to muscle thin filaments. *J. Mol. Biol.* 147:297–324.
25. Unwin, P. N. T., and R. Henderson. 1975. Molecular structure determination by electron microscopy of unstained crystalline specimens. *J. Mol. Biol.* 94:425–440.
26. Wakabayashi, T., H. E. Huxley, L. A. Amos, and A. Klug. 1975. Three-dimensional image reconstruction of actin-tropomyosin complex and actin-tropomyosin-troponin T-troponin I complex. *J. Mol. Biol.* 93:477–497.
27. Wrigley, N. G. 1968. The lattice spacing of crystalline catalase as an internal standard of length in electron microscopy. *J. Ultrastruct. Res.* 24:454–464.